RSC Advances

PAPER

View Article Online
View Journal | View Issue

Cite this: *RSC Adv.*, 2022, **12**, 27116

Highly sensitive and selective colorimetric detection of Pb(II) ions using *Michelia tonkinensis* seed extract capped gold nanoparticles

Bao An Huynh,[a] Van-Dat Doan, *[a] Van Cuong Nguyen, [a] Anh-Tien Nguyen[b] and Van Thuan Le *[cd]

In this study, gold nanoparticles (AuNPs) were synthesized *via* a green and environmentally-friendly approach and applied as a colorimetric probe for detecting Pb^{2+} ions in aqueous solution. Instead of toxic chemicals, *Michelia tonkinensis* (MT) seed extract was used for reducing Au^{3+} and stabilizing the formed AuNPs. The synthesis conditions, including temperature, reaction time, and Au^{3+} ion concentration, were optimized at 90 °C, 40 min, and 1.25 mM, respectively. The physicochemical properties of the produced MT-AuNPs were assessed by means of transmission electron microscopy, X-ray diffraction, field emission scanning electron microscopy, dynamic light scattering, and Fourier-transform infrared spectroscopy. The characterization results revealed that the MT-AuNPs exhibited a spherical shape with a size of about 15 nm capped by an organic layer. The colorimetric assay based on MT-AuNPs showed excellent sensitivity and selectivity toward Pb^{2+} ions with the limit of detection value of 0.03 μM and the limit of quantification of 0.09 μM in the linear range of 50–500 μM. The recoveries of inter-day and intra-day tests were 97.84–102.08% and 98.78–102.34%, respectively. The MT-AuNPs probe also demonstrated good and reproducible recoveries (98.71–101.01%) in analyzing Pb^{2+} in drinking water samples, indicating satisfactory practicability and operability of the proposed method.

Received 9th August 2022
Accepted 19th September 2022

DOI: 10.1039/d2ra04981c

rsc.li/rsc-advances

1. Introduction

Lead (Pb) is a persistent heavy metal with extremely high toxicity to cells and the nervous system. It can cause cancer and mutations in humans and animals even at low concentrations. Pb is commonly found in wastewater from batteries, fuel additives and electronic accessories manufacturing plants.[1] Delays in the detection and quantification of Pb^{2+} in water bodies can lead to serious health and environmental problems.

There are many methods available for the determination of Pb^{2+}, including inductively coupled plasma-atomic emission spectrometry, atomic absorption spectrometry, electrochemical methods, and inductively coupled plasma mass spectrometry.[2,3] However, these methods often require expensive instruments and complex operations. These limitations have prevented their widespread application for rapid and trustable analysis of various substances. Meanwhile, colorimetric sensing methods have expressed great potential for the detection of metallic ions and toxic pollutants on account of their quick detection, naked-eye sensing, high sensitivity, and easy fabrication.[4]

The advent of nanotechnology has created a huge leap forward in materials science. With unique properties, nanomaterials have been widely applied in medicine, optics, environmental treatment, catalysis, and electronic devices.[5,6] Recently, nanomaterials have also been extensively used to fabricate different sensors for detecting heavy metals in aqueous solutions owing to their strong surface Plasmon resonance (SPR) and ease of functionalization.[7,8] Among them, gold nanoparticles (AuNPs) have received the most attention because of their high-performance sensing, environmental friendliness, tunable properties and photostability.[9] Several colorimetric sensors based on AuNPs have been designed for the quantitative analysis of different heavy metals such as Hg^{2+},[10] Fe^{3+},[11] Al^{3+},[12] Cd^{2+},[13] and Pb^{2+} ions[14,15].

In recent years, green approaches using aqueous plant extracts for nanoparticles synthesis have attracted much attention in terms of their simplicity, environmental safety, and low cost.[16,17] Plants often contain several secondary metabolites, such as flavonoids, alkaloids, steroids, saponins, tannins, and phenolic acids, which can act as both reducing and stabilizing agents in plant-mediated synthesis.[18] More importantly, these compounds possess various biological activities, including antioxidant, anticancer, antiviral, and antibacterial properties.[19]

[a]*Faculty of Chemical Engineering, Industrial University of Ho Chi Minh City, Ho Chi Minh City, 700000, Vietnam. E-mail: doanvandat@iuh.edu.vn*

[b]*Faculty of Chemistry, Ho Chi Minh City University of Education, 280 An Duong Vuong, Ho Chi Minh City, 700000, Vietnam*

[c]*Center for Advanced Chemistry, Institute of Research & Development, Duy Tan University, 03 Quang Trung, Danang City, 550000, Vietnam. E-mail: levanthuan3@duytan.edu.vn*

[d]*The Faculty of Natural Sciences, Duy Tan University, 03 Quang Trung, Da Nang, 550000, Vietnam*

Therefore, the nanoparticles prepared with plant extracts exhibit high biocompatibility, stability, and safety in medical and environmental applications.

Many species of plant, including *Phragmites australis* root,[20] *Limnophila rugosa* leaves,[21] *Lactuca indica* leaf,[22] *Annona squamosa*,[23] and *Codonopsis pilosula* root,[24] *etc.*, have been successfully utilized to synthesize AuNPs. It should be noted that differences in plant composition can lead to diverse properties of the novel metallic AuNPs. Besides, it is also indicated that the selectivity and sensitivity of these sensors largely depended on the surface denaturation of AuNPs.[25] Therefore, new plants are always sought to fabricate AuNPs.

Michelia tonkinensis (MT) is a member of the *Magnoliaceae* family distributed mainly in Vietnam and China. This plant is used for wood, seeds (spice) and medicine.[26] MT seed extract is rich in essential oils with numerous active groups, so it is used for treating flu, malaria, and infections.[27] Besides, these bioactive compounds can play a crucial role in the reduction of metal ions to nanoparticles. To our knowledge, the use of the MT extract as a green reducing agent for the synthesis of AuNPs has not been mentioned.

In this regard, the present work offers a simple, eco-friendly method using the aqueous extract of MT seeds as a bioreductant and stabilizer for the synthesis of AuNPs (denoted as MT-AuNPs), which are used as a colorimetric sensor for the rapid detection of Pb^{2+} ions in aqueous solution. The optimization of synthesis conditions and characterization of MT-AuNPs were performed. The selectivity and sensitivity of the MT-AuNPs probe were established. Furthermore, the practicality of the proposed assay was verified through testing Pb^{2+} ions in drinking water samples. The developed colorimetric sensor displayed a low detection limit (LOD) of 0.03 μM, which is more sensitive than many reported methods.

2. Materials and methods

2.1. Materials

All reagents and chemicals used in this study were used directly, with no further purification. Tetrachloroauric acid ($HAuCl_4 \cdot 3H_2O$, ≥ 99.9%) were purchased from Acros Organics (Belgium). Lead(II) nitrate ($Pb(NO_3)_2$, ≥ 99%) and other metal were obtained from Beijing Chemical Company (Beijing, China). MT seeds were collected in Ha Giang province of Vietnam and sun-dried until the moisture content was about 10%.

2.2. Preparation of *Michelia tonkinensis* seeds extract

The dried MT seeds were ground to a fine powder before extraction. The MT extract was obtained by stirring 10 g of MT powder with 450 mL of distilled water at 100 °C for 1 h. The MT residue was then removed by filtration and the extract was stored in a refrigerator at 4–8 °C.

2.3. Biosynthesis of AuNPs

The AuNPs samples were photosynthesized by mixing $HAuCl_4$ solution and aqueous MT extract at a volume ratio of 1 : 1 in the dark. The synthesis parameters such as Au^{3+} concentration, reaction time and temperature were varied and their effect on the formation of AuNPs was monitored to establish the optimal synthesis conditions. The successful synthesis of MT-AuNPs was confirmed by the color change of the MT solution, and was monitored using a UV-vis spectrophotometer (Evolution 300, Germany) with characteristic absorbance at around 540 nm. The MT-AuNPs samples obtained at optimal conditions were centrifuged, dried, and characterized by various techniques.

2.4. Characterization of biogenic of MT-AuNPs

The chemical bonds of functional groups in the MT extract and powdered MT-AuNPs were investigated using Fourier transform infrared spectroscopy (FTIR) on a Bruker Tensor 27 (Germany). The powder X-ray diffraction (XRD) analysis was performed on a Shimadzu 6100 X-ray (Japan) diffractometer (voltage = 40 kV, current = 30 mA, $\lambda_{CuK\alpha}$ = 1.5406 Å) to determine the crystal structure and phase composition. The zeta potential and size distribution of MT-AuNPs in colloidal solution were measured on a Horiba SZ-100 instrument (Japan). The morphology of AuNPs crystals in colloidal solution was studied using a Tecnai G2 20 S-TWIN (Japan) transmission electron microscope (TEM). The morphology of the MT-AuNPs powder was observed by a field-emission scanning electron microscope (FE-SEM, Hitachi S-4800, Japan). A dispersive energy X-ray (EDX) spectroscopy was conducted on a Horiba EMAX Energy EX-400 analyzer (Japan) to determine the chemical elemental composition of the MT-AuNPs samples.

2.5. Detection of Pb^{2+} ions

The MT-AuNPs colloidal solution prepared at optimal conditions was further used as a colorimetric sensor for the detection of several environmentally important metal ions. Briefly, a series of metal ions (Cu^{2+}, Fe^{2+}, Mn^{2+}, Mg^{2+}, Ca^{2+}, Pb^{2+}, Cr^{3+}, Al^{3+}, Ba^{2+}, Ni^{2+}, Ti^{2+}, Cd^{2+}, Fe^{3+}, and Zn^{2+}) at a concentration of 1000 μM were separately added to the MT-AuNPs solution with a volume ratio of 1 : 2. After incubation for 5 min, the UV-vis spectra of the mixtures were recorded on a Cary 60 UV-Vis spectrophotometer (Agilent, USA) in the wavelength range of 200–800 nm. The selectivity of the MT-AuNPs probe was evaluated through the change of the SPR band and the color of the mixture.

In order to quantify Pb^{2+} ions, different concentrations (0–5000 μM) of Pb^{2+} were incubated with the MT-AuNPs solution for 5 min and measured the intensity of the SPR band. Next, a calibration curve was established based on the relationship between the relative absorbance ($(A_0 - A)/A_0$) and the Pb^{2+} concentration. The detectable linear range was further determined by applying a linear regression method.

The effect of salt concentration on the sensor response was checked in the presence of NaCl and CH_3COONa. The mixtures of Pb(II) and salt solutions were prepared with a fixed Pb(II) concentration of 400 μM and a variable salt concentration (0, 40, 60, 80, 100, 120, 140, 160, and 200 mM). Then, the prepared solutions were incubated with the MT-AuNPs colloid in the ratio 1 : 2 for 5 min. After that, the UV-vis spectra of the resulting

mixture was recorded. The MT-AuNPs without Pb(II) were also tested in the same way for comparison.

The inter-day and intra-day tests were also performed to estimate the precision and accuracy of the designed sensor. Three standard solutions of Pb(II) with concentrations of 100, 200 and 400 μM were used for testing. The Pb(II) analysis by the MT-AuNPs assay was carried out five times in a day (intra-day test) and once a day for three days (inter-day test). The precision (expressed as the percentage of relative standard deviation (% RSD)) and accuracy (the recovery percentage (%)) were calculated according to the following formula.

$$\%\ \mathrm{RSD} = (\text{standard deviation/mean}) \times 100 \quad (1)$$

$$\text{Recovery}\ (\%) = (\text{mean of determined value/theoretical value}) \times 100 \quad (2)$$

The practical applicability of the detection system has been verified by analyzing Pb^{2+} concentration in drinking water samples. A calculated amount of Pb^{2+} was initially spiked to the drinking water (bottled water, Aquafina), and MT-AuNPs were then added to the mixture.[8] After 5 min, the absorbance of the tested samples was measured at 545 nm to calculate the Pb^{2+} concentration using the determined linear equation. Finally, the recovery was assessed by the equation: (found concentration)/(added concentration) × 100%. For comparison, the Pb(II) concentration in the testing samples (without MT-AuNPs) was rechecked by the atomic absorption spectroscopy method (AAS) on an iCE 3500 analyzer (Thermo Scientific, Germany). The measurements were repeated at least three times and averaged.

3. Results and discussion

3.1. Synthesis of MT-AuNPs

The effects of reaction time, temperature and Au^{3+} concentration on the formation of the metallic nanoparticles were investigated in order to establish the best synthesis conditions. The optimal conditions were selected based on two key factors, involving the high concentration and stability of the nanoparticle solutions obtained.[7] The experiments were conducted by changing the survey parameter while keeping the remaining

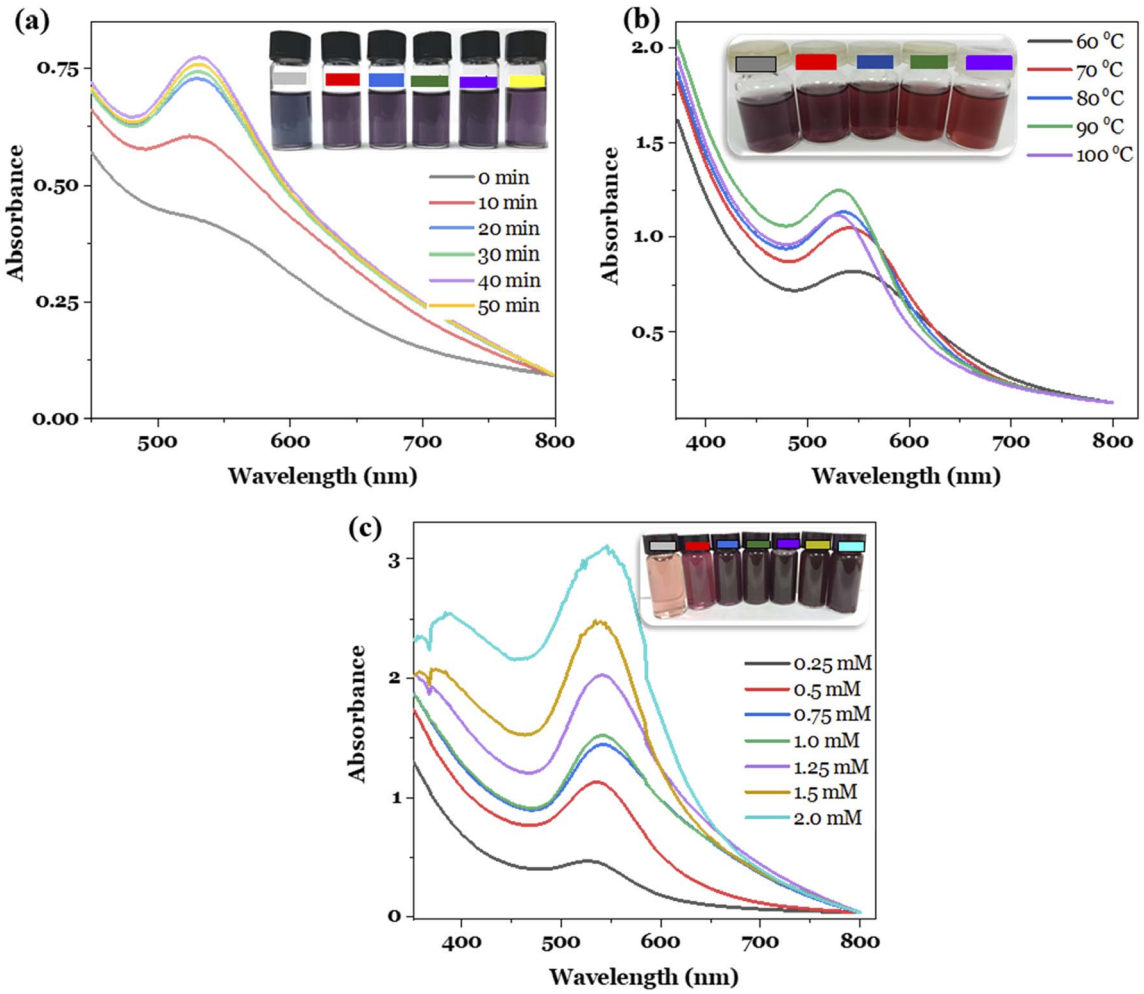

Fig. 1 Optimization of synthesis conditions: (a) reaction time ($[Au^{3+}] = 1.0$ mM, $T = 80$ °C), (b) reaction temperature ($[Au^{3+}] = 1.0$ mM, $t = 40$ min), and (c) Au^{3+} concentration ($T = 90$ °C, $t = 40$ min).

conditions constant. For investigating the reaction time, the conditions were established as follows: Au^{3+} concentration of 1.0 mM, reaction temperature of 80 °C, the Au^{3+}/MT extract volume ratio of 1 : 1, and reaction time of 0, 10, 20, 30, 40, and 50 min. The study result is presented in Fig. 1a. It can be seen that the obtained MT-AuNPs solutions had a characteristic purple color and provided the SPR peak at 540 nm. Furthermore, the intensity of the SPR band increased with rising reaction time, probably due to the increased number of AuNPs formed. However, when the reaction time exceeded 50 min, the SPR absorbance decreased, and the nano-system became less stable over time by reason of the agglomeration of metallic nanoparticles.[28] Therefore, the synthesis time of 40 min was chosen for the further synthesis of MT-AuNPs.

The effect of reaction temperature was studied in the range of 60–100 °C with Au^{3+} ion concentration of 1.0 mM and a reaction time of 40 min. The results depicted in Fig. 1b revealed that the reaction temperature had a significant influence on the formation of nanoparticles. With raising the temperature, the intensity of the SPR peak increased and reached the highest value at 90 °C, and then decreased at higher temperatures. The observed tendency could be related to the fact that high temperatures provided more energy to the reacting molecules, increasing the reaction efficiency. However, too high temperatures also increased the frequency of collisions between particles, leading to their agglomeration and coagulation.[21] Notably, at reaction temperatures higher than 80 °C, the SPR peak shifted from 540 nm to 530 nm, along with the color of the MT-AuNPs solution changing from purple to brown due to the change in nanoparticle size. This finding demonstrated that the temperature affected the morphology of AuNPs. Similar results were observed for the synthesis of AuNPs using the *Cistanche deserticola* extract.[29] Therefore, 90 °C was selected as the optimal temperature for the MT-AuNP synthesis.

Finally, the metal ion amount influence was checked by varying the Au^{3+} concentration from 0.25 to 2.0 mM, while the reaction time and temperature were kept at optimal values. As shown in Fig. 1c, the higher the concentration of Au^{3+} supplied to the reaction, the higher the efficiency of AuNPs formation. However, at concentrations higher than 1.5 mM, the SPR peaks became noisy, and the resulting MT-AuNPs solutions were also less stable. This phenomenon may be due to the insufficient amount of extract to stabilize the nanoparticles and the excess Au^{3+} ions that were then adsorbed onto the surface of AuNPs, reducing the zeta potential and increasing the agglomeration.[28] Hence, the Au^{3+} concentration of 1.25 mM was considered suitable for the synthesis of MT-AuNPs.

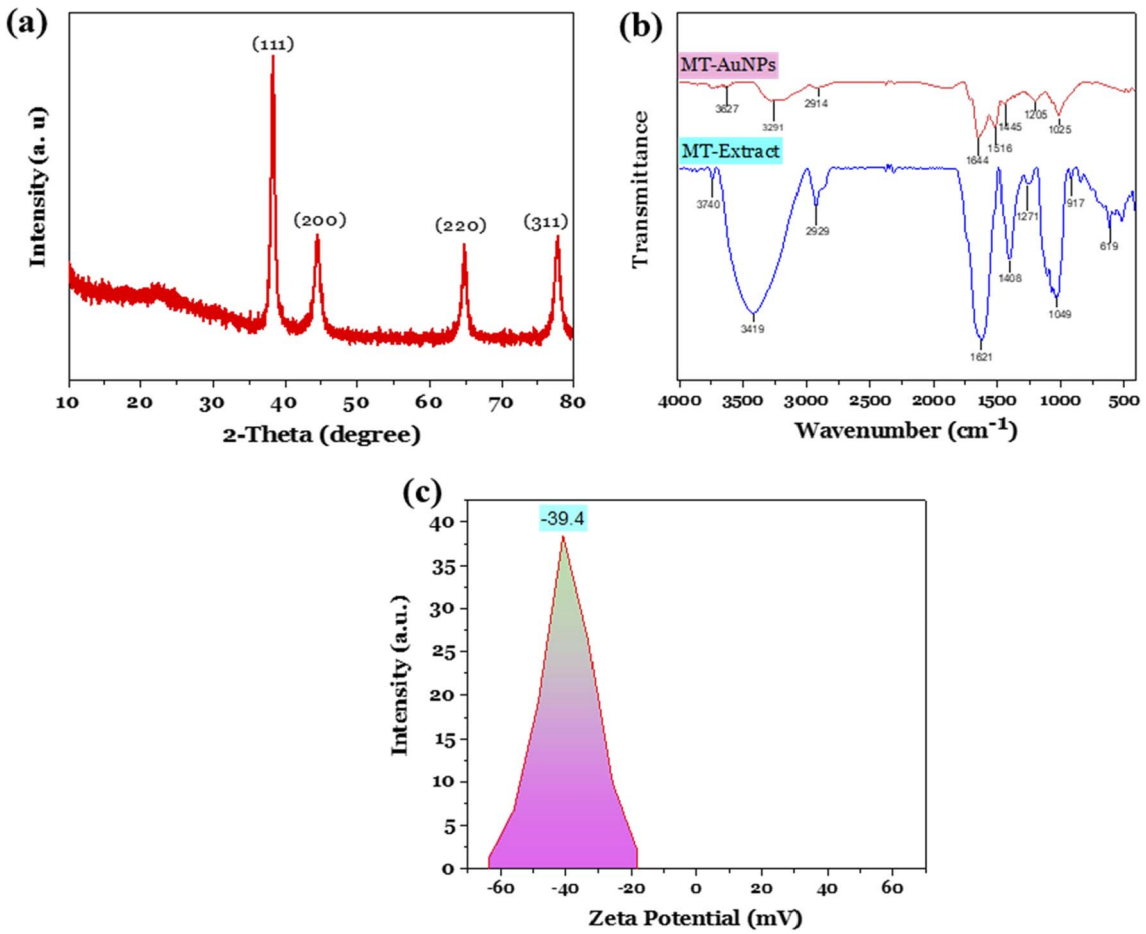

Fig. 2 XRD pattern (a), FTIR spectra (b), and zeta potential (c) of MT-AuNPs.

3.2. Characterization of MT-AuNPs

The MT-AuNPs samples produced at optimal conditions were characterized by XRD, FE-SEM, TEM, DLS, and EDX techniques. Fig. 2a shows the XRD pattern of MT-AuNPs with the appearance of four characteristic peaks at $2\theta = 38.25°$, 44.41°, 64.71°, and 77.64°, corresponding to the face-centered cubic lattice planes of metallic gold (111), (200), (220), and (311) (ICDD PDF card number 00-004-0784).[30] The highest diffraction peak at 2θ of 38.25° demonstrated that the AuNPs crystals preferentially grew in the direction of the Miller index plane of (111). The average crystal size d (nm) was further calculated by the Debye–Scherrer equation $d = 0.9\lambda/\beta \cos\theta$, where β (radian) is the full width at half peak, λ (0.1540 nm) is the wavelength of the CuKα, and θ (degrees) denotes the Bragg diffraction angle. As a result, the average crystal size of MT-AuNPs was found to be 16.2 nm.

The presence of functional groups in both MT seed extract and MT-AuNPs surface was investigated using FTIR spectroscopy (Fig. 2b). The FTIR spectrum of MT seed extract and its AuNPs showed similar absorbance bands at around 3419, 2929, 1621, 1408, and 1271 cm^{-1}, which were attributed to the O–H, C–H, C=C, C=O, and N–H stretching vibrations, respectively.[24,27,31] The similarity of the FTIR spectra indicated the existence of an organic layer on the surface of AuNPs, which resisted nanoparticle agglomeration and ensured the stability of the colloidal system.[32] In addition, the shift of FTIR peaks of MT-AuNPs compared with MT extract was also observed, and this possibly was due to the interaction of functional groups with the AuNPs surface. The formation of the protective layer around AuNPs can be described as follows. After participating in the Au^{3+} reduction process, the phytoconstituents of MT extract adsorbed onto the surface of AuNPs, creating a negatively charged organic layer that hindered coagulation *via* electrostatic repulsion. The negative charge of MT-AuNPs surface is due to the presence of negatively charged oxygen-containing groups such as OH^-, COO^{-}.[8] Indeed, the actual results obtained show that the zeta potential of MT-AuNPs at pH of 5.5 was −39.4 mV (Fig. 2c), which was noteworthy higher than that of AuNPs prepared using *Sargassum carpophyllum* (−0.047 mV) and *Crinum latifolium* leaf extract (−20.8 mV), suggesting excellent long-term stability of MT-AuNPs solution.

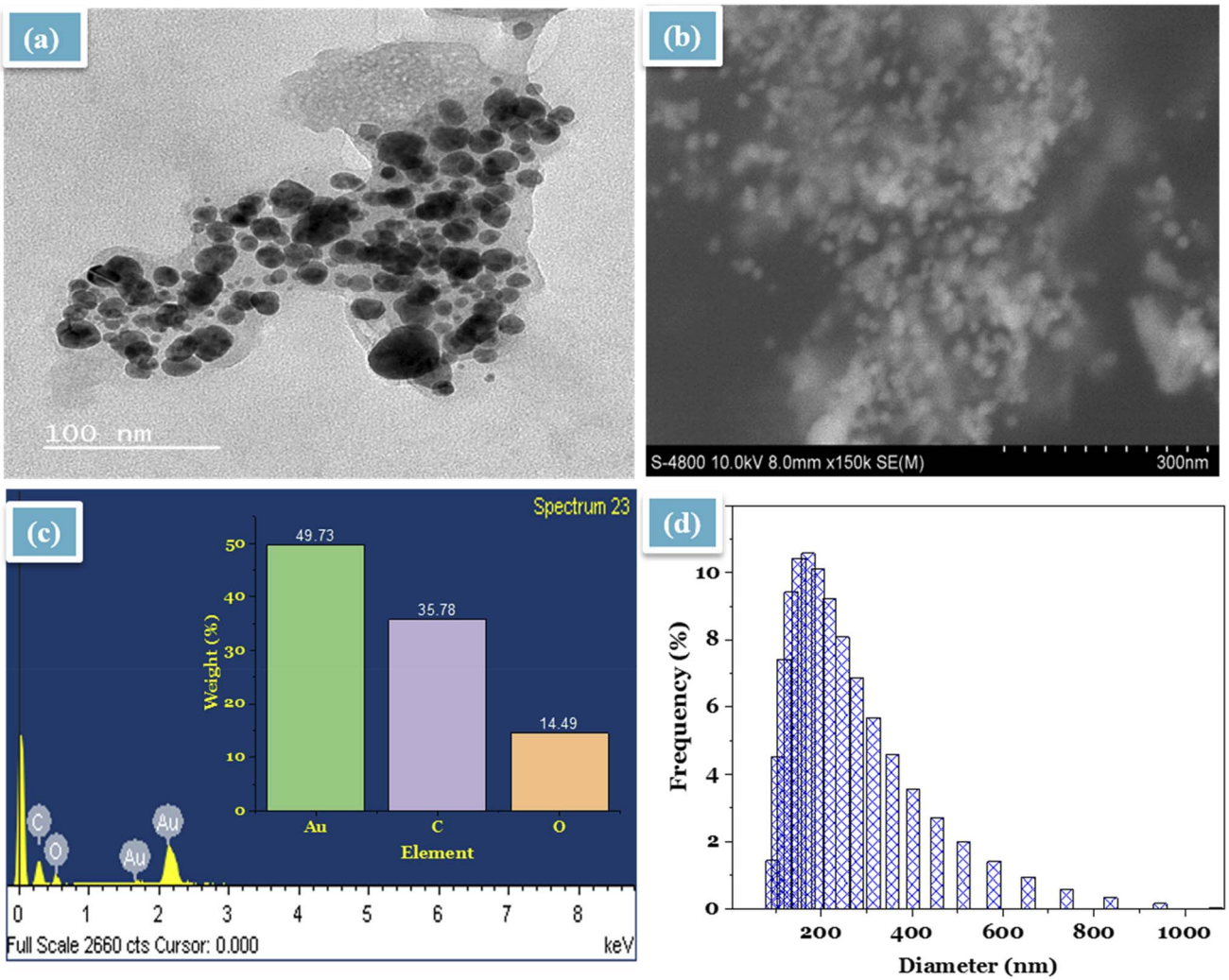

Fig. 3 TEM (a) and SEM (b) images, EDX spectrum (c), and DLS (d) of MT-AuNPs.

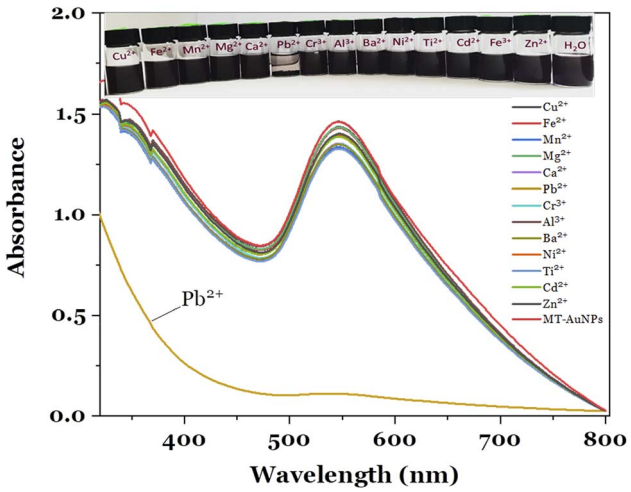

Fig. 4 Selectivity of the MT-AuNPs probe with different metal ions.

The morphology of the synthesized MT-AuNPs in the colloidal and powder phase was investigated by TEM and SEM, respectively. According to TEM image (Fig. 3a), MT-AuNPs crystals were spherical with an average diameter of about 15 nm and evenly distributed. Meanwhile, the SEM image (Fig. 3b) showed that the shape and size of MT-AuNPs in the powder phase were similar to those of the TEM result. It should be noted that MT-AuNPs were distributed separately due to the capped organic layer. Furthermore, EDX analysis revealed that the produced metallic nanoparticles contained mainly Au, C and O elements with percentage compositions of 49.73, 35.78, and 14.49%, respectively. The presence of C and O in the sample was related to the organic molecules responsible for stabilizing the metallic nanoparticles. Similar results were also observed when synthesizing AuNPs from several plant extracts.[15,21,24,28] Further, the DLS study was performed to calculate the size of MT-AuNPs in aqueous solution. As illustrated in Fig. 3d, the size of MT-AuNPs was distributed in the range of 75–950 nm with an average diameter of 190 nm. Because the DLS technique measures the hydrodynamic diameter of the particles, it gave a larger size of MT-AuNPs than the results from TEM, SEM, and XRD.

3.3. Colorimetric detection of Pb^{2+}

The fabricated MT-AuNPs were further used as a colorimetric sensor for metal ions detection. The selectivity of the designed

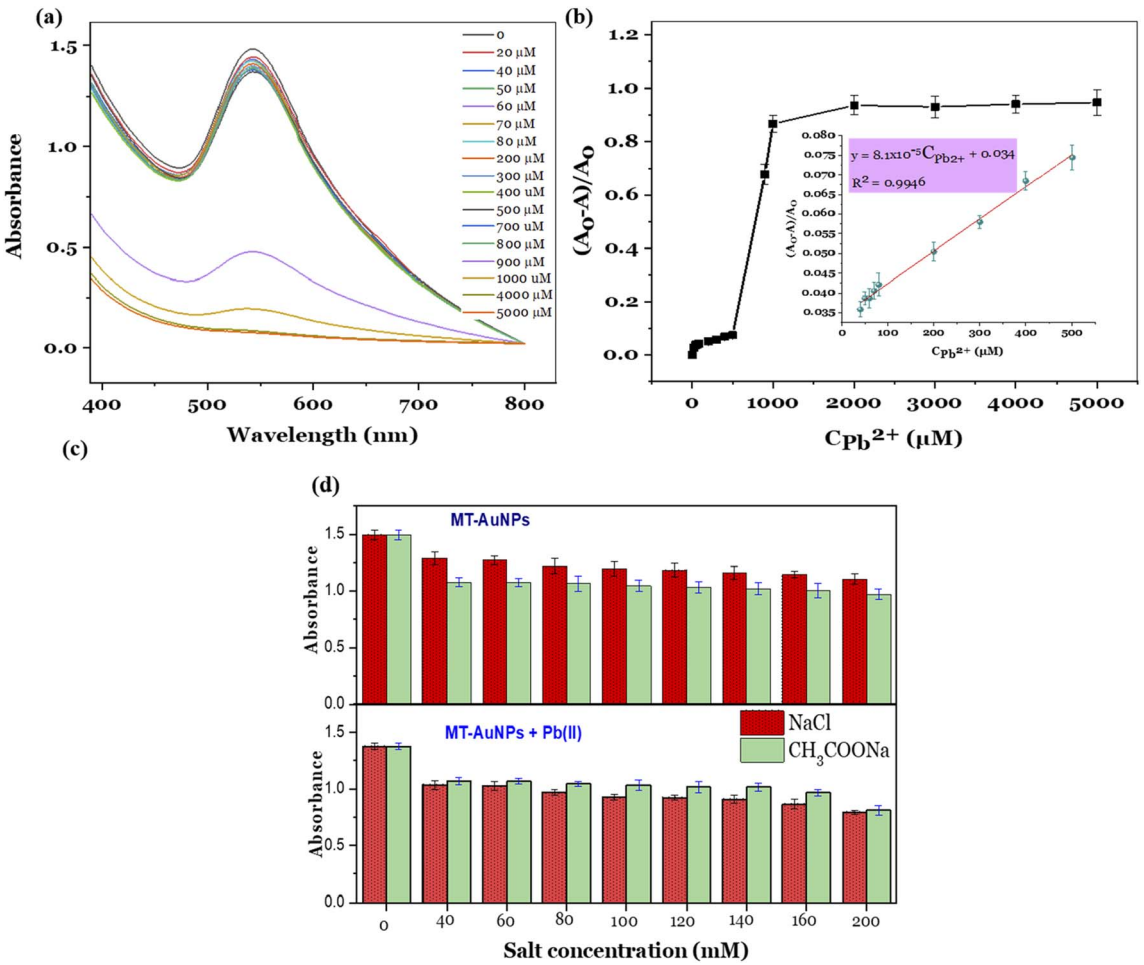

Fig. 5 (a) UV-vis measurements of different Pb^{2+} concentrations with MT-AuNPs, (b) plot of relative absorbance *versus* Pb^{2+} concentrations, and (c) effect of salt concentration on the SPR absorbance of the MT-AuNPs solution without and with Pb(II) ions.

Table 1 A comparison of various colorimetric detection methods for detection of Pb(II)

Materials	Linear range (μM)	LOD (μM)	Ref.
Siraitia grosvenorii–AuNPs	0–1000	0.018	8
L-tyrosine–AuNPs	0.02–0.1	0.016	33
Valine capped AuNPs	1–100	30.5	34
SiO_2@Au NCs	0.5–50	0.05	35
2-Mercaptoisonicotinic acid functionalized AuNPs	0.34–0.67	0.1	36
GSH-AuNPs	0.1–30	0.1	37
MT-AuNPs	50–500	0.03	This work

sensor was investigated with various cations, including Cu^{2+}, Fe^{2+}, Mn^{2+}, Mg^{2+}, Ca^{2+}, Pb^{2+}, Cr^{3+}, Al^{3+}, Ba^{2+}, Ni^{2+}, Ti^{2+}, Cd^{2+}, and Zn^{2+}. The test results are depicted in Fig. 4.

It can be seen that the MT-AuNPs assay exhibited the highest selectivity toward Pb^{2+} ions. The evidence for this claim was that the intensity of the SPR band of MT-AuNPs strongly decreased and almost disappeared when Pb^{2+} was added, whereas it changed only slightly with the introduction of other metals. Besides, the Cu^{2+}, Fe^{2+}, Mn^{2+}, Mg^{2+}, Ca^{2+}, Cr^{3+}, Al^{3+}, Ba^{2+}, Ni^{2+}, Ti^{2+}, Cd^{2+}, and Zn^{2+} cations had no obvious effect on the color of MT-AuNPs as compared to Pb^{2+}, which made the solution lose its purple color under the same conditions. The decrease in color intensity of the colloidal solution with the presence of Pb^{2+} was due to the agglomeration of MT-AuNPs (inset in Fig. 4), which was caused by the formation of complexes between Pb^{2+} and biomolecules adsorbed on the AuNPs surface.[8] The obtained result confirmed that the agglomeration was the dominant mechanism of the proposed colorimetric probe.

The quantitative detection of Pb^{2+} was carried out using the standard curve method. For establishing the calibration curve, various concentrations of Pb^{2+} ions in the range of 0–5000 μM were added in the MT-AuNPs solutions, and the UV-vis spectra of the resulting mixture were recorded. As presented in Fig. 5a, the intensity of the SPR band gradually decreased with increasing Pb^{2+} concentration from 20 to 800 μM and declined sharply when the Pb^{2+} concentration was higher than 800 μM. High Pb^{2+} concentrations led to a high degree of coagulation, resulting in the rapid reduction in the SPR intensity. In this case, the concentration of 800 μM can be served as a coagulation threshold. The calibration curve was then constructed by plotting the relative absorbance ($(A_0 - A)/A_0$) against Pb^{2+} concentration, where A_0 and A are the absorbances of SPR band (540 nm) without Pb^{2+} and with the presence of Pb^{2+}, respectively. The relationship between the relative absorbances and the Pb^{2+} concentration is illustrated in Fig. 5b. From the Fig. 5b, the detectable linear range was determined to be 0–500 μM with the regression equation of $(A_0 - A)/A_0 = 8.1 \times 10^{-5}\, C_{Pb^{2+}} + 0.034$ and correlation coefficient $R^2 = 0.9946$ (insert in Fig. 5b). The limit of detection (LOD) and the limit of quantitation (LOQ) were calculated based on the slope and standard deviation of the analytical response (LOD $= 3\sigma/S$ and LOQ $= 10\sigma/S$) (σ is the standard deviation and S is the slope of the calibration curve). The LOD and LOQ values for the MT-AuNPs sensor were found to be 0.03 μM (6.21 μg L^{-1}) and 0.09 μM (18.63 μg L^{-1}). Notably, the LOD of MT-AuNPs meets the mandatory upper limit of the World Health Organization (10 μg L^{-1}) for Pb^{2+} in drinking water. Furthermore, compared to other colorimetric sensors (listed in Table 1), the MT-AuNPs probe possessed a relatively low LOD, suggesting that MT-AuNPs could be used as a promising assay for the quantitative analysis of Pb^{2+} detection.

The presence of salt in the test sample can influence the aggregation of nanoparticles, affecting the response of the sensor. In this study, NaCl and CH_3COONa were selected as an example to describe the experiment. The MT-AuNPs solution without and with Pb(II) ions were respectively incubated with various concentrations of salts and their UV-vis spectra were recorded. Fig. 5c shows effect of salt concentration on the SPR absorbance of the MT-AuNPs solution without (top panel) and with Pb(II) ions (lower panel). It can be seen that the used salts have an effect on the agglomeration of MT-AuNPs, leading to a decrease in the intensity of the SPR peak for both solutions with and without Pb(II). This phenomenon is commonly observed in many studies and is thought to be related to the decrease in the zeta potential value of the nanoparticles in the presence of salt ions.[38] With increasing concentration of NaCl and CH_3COONa from 40 to 200 mM, the agglomeration degree tended to increase. However, this increase was very slight, indicating that the effectiveness of the salt concentration in

Table 2 Recovery and precision determined from inter-day and intra-day tests

	Concentration (μM)					
	100		200		400	
Method	RSD %	Recovery %	RSD %	Recovery %	RSD %	Recovery %
Inter-day	1.6	97.84 ± 1.03	3.7	98.97 ± 2.11	1.9	102.08 ± 1.73
Intra-day	2.3	98.78 ± 0.92	2.8	102.34 ± 0.87	4.1	101.29 ± 1.25

Table 3 Determination of Pb^{2+} in drinking water samples using MT-AuNPs and AAS

Sample	Added concentration (μM)	Found concentration (μM)		Recovery (%)
		MT-AuNPs assay	AAS	
1	0	0	0	
2	50	49.10 ± 0.57	49.64 ± 0.91	101.01
3	100	98.71 ± 2.15	100.08 ± 0.82	98.71
4	250	248.72 ± 1.03	249.07 ± 0.78	99.49
5	350	351.80 ± 0.93	350.82 ± 0.35	100.51

causing aggregation was low. For the MT-AuNPs samples, CH_3COONa appeared to be slightly more effective in causing aggregation compared to NaCl. This is probably due to that CH_3COO^- ions have higher affinity to AuNPs. However, the opposite trend was observed for MT-AuNPs with the presence of Pb(II). The obtained result could be related to the possibility of precipitation between Cl^- and Pb(II) ions. Therefore, the presence of salt is not useful for this colorimetric sensing method. To improve the accuracy of the method, it is necessary to remove the salts from the solution before analysis.

In order to verify the repeatability of the proposed probe, three concentration levels (100, 200, and 400 μM) were analyzed to determine the precision and recovery of Pb(II). The precision and recovery of the MT-AuNPs assay for Pb(II) are shown in Table 2. The results of the inter-day and intra-day tests demonstrated high reproducibility of the MT-AuNPs sensor, with RSD of the intra-day and inter-day analysis ranging between 2.3–4.1% and 1.6–3.7%, respectively. The recoveries of inter-day and intra-day tests were 97.84–102.08% and 98.78–102.34%, respectively. Therefore, the validated method can be sever as a promoting colorimetric sensor for monitoring Pb(II) concentration in aqueous solution.

The practical applicability of the proposed method was tested with drinking water samples injected with Pb^{2+} standard solutions, and the results are summarized in Table 3. As presented in Table 3, the Pb(II) analysis results measured by the MT-AuNPs sensor were not remarkably different from the AAS method. Moreover, the recoveries of the MT-AuNPs probe for the detection of Pb^{2+} ions in testing samples were high, ranging from 98.71% to 101.01%, validating the great practicality of MT-AuNPs for checking Pb^{2+} ions in real water samples.

4. Conclusions

The present study provided a green and simple approach for producing AuNPs using MT seed extract. The synthesis conditions were optimized with the reaction time, temperature, and metal ion concentration of 40 min, 90 °C, and 1.25 mM, respectively. The XRD and TEM analysis confirmed the successful synthesis of spherical MT-AuNPs with an average size of about 15 nm. MT-AuNPs presented high stability due to possessing a high zeta potential value (−39.4 mV). The colorimetric probe based on MT-AuNPs exhibited excellent selectivity and sensitivity towards Pb^{2+} ions. This assay can achieve LOD of 0.03 μM and LOQ of 0.09 μM in the linear range of 0–500 μM. The feasibility of the proposed method for Pb^{2+} ion analysis in real water systems was confirmed by the high recoveries of 98.71–101.01%. Overall, the findings indicated that the developed MT-AuNPs material could be successfully utilized as a colorimetric sensor for the detection of Pb^{2+} from both drinking and real water samples.

Author contributions

Bao An Huynh: investigation, methodology, writing original draft. Van-Dat Doan: formal analysis, visualization, resources, investigation, writing-review & editing. Van Cuong Nguyen: methodology, data curation. Anh-Tien Nguyen: investigation, data analysis. Van Thuan Le: conceptualization, methodology, writing-review & editing, supervision.

Conflicts of interest

There are no conflicts to declare.

References

1 F. Li, Z.-H. Liu, X. Tian, T. Liu, H.-L. Wang and G. Xiao, *J. Funct. Foods*, 2020, **75**, 104201.
2 S. Takahashi, H. Yanagisawa, T. Kamata, D. Kato, R. Kurita, S. Shiba and O. Niwa, *Bunseki Kagaku*, 2021, **70**, 101–109.
3 I. P. Paktsevanidou, N. Manousi and G. A. Zachariadis, *Anal. Lett.*, 2021, **54**, 2227–2238.
4 B. Sahu, R. Kurrey, M. K. Deb, K. Shrivas, I. Karbhal and B. R. Khalkho, *RSC Adv.*, 2021, **11**, 20769–20780.
5 V.-D. Doan, T. L. Phan, V. T. Le, Y. Vasseghian, L. O. Evgenievna, D. L. Tran and V. T. Le, *Chemosphere*, 2022, **286**, 131894.
6 H. R. Rajabi, M. Shamsipur, A. A. Khosravi, O. Khani and M. H. Yousefi, *Spectrochim. Acta, Part A*, 2013, **107**, 256–262.
7 T. H. Anh Nguyen, V.-C. Nguyen, T. N. Huynh Phan, V. T. Le, Y. Vasseghian, M. A. Trubitsyn, A.-T. Nguyen, T. P. Chau and V.-D. Doan, *Chemosphere*, 2021, **287**, 132271.
8 V. T. Le, T. G. Duong, V. T. Le, T. L. Phan, T. L. Huong Nguyen, T. P. Chau and V.-D. Doan, *RSC Adv.*, 2021, **11**, 15438–15448.
9 S. Mirsadeghi, H. Zandavar, M. Yousefi, H. R. Rajabi and S. M. Pourmortazavi, *J. Environ. Manage.*, 2020, **270**, 110831.
10 Y. Hu, Z. Huang, B. Liu and J. Liu, *ACS Appl. Nano Mater.*, 2021, **4**, 1377–1384.

11 T. T.-T. Ho, C.-H. Dang, T. K.-C. Huynh, T. K.-D. Hoang and T.-D. Nguyen, *Carbohydr. Polym.*, 2021, **251**, 116998.
12 N. Garg, S. Bera and A. Ballal, *Spectrochim. Acta, Part A*, 2020, **228**, 117701.
13 Y. Gan, T. Liang, Q. Hu, L. Zhong, X. Wang, H. Wan and P. Wang, *Talanta*, 2020, **208**, 120231.
14 Y. Cai, B. Ren, C. Peng, C. Zhang and X. Wei, *Molecules*, 2021, **26**, 3180.
15 B. Feng, R. Zhu, S. Xu, Y. Chen and J. Di, *RSC Adv.*, 2018, **8**, 4049–4056.
16 S. Mirsadeghi, F. M. Koudehi, R. H. Rajabi and M. S. Pourmortazavi, *Curr. Pharm. Biotechnol.*, 2020, **21**, 1129–1137.
17 H. R. Rajabi, F. Sajadiasl, H. Karimi and Z. M. Alvand, *J. Mater. Res. Technol.*, 2020, **9**, 15638–15647.
18 V.-D. Doan, A. T. Thieu, T.-D. Nguyen, V.-C. Nguyen, X.-T. Cao, T. L.-H. Nguyen and V. T. Le, *J. Nanomater.*, 2020, **2020**, 1–10.
19 Z. Moradi Alvand, H. R. Rajabi, A. Mirzaei, A. Masoumiasl and H. Sadatfaraji, *Mater. Sci. Eng., C*, 2019, **98**, 535–544.
20 M. Hosny, M. Fawzy, O. M. El-Borady and A. E. D. Mahmoud, *Adv. Powder Technol.*, 2021, **32**, 2268–2279.
21 V. T. Le, N. N. Q. Ngu, T. P. Chau, T. D. Nguyen, V. T. Nguyen, T. L. H. Nguyen, X. T. Cao and V. Doan, *J. Nanomater.*, 2021, **2021**, 1–11.
22 T. T. Vo, C. H. Dang, V. D. Doan, V. S. Dang and T. D. Nguyen, *J. Inorg. Organomet. Polym. Mater.*, 2020, **30**, 388–399.
23 L. K. Ruddaraju, P. N. V. K. Pallela, S. V. N. Pammi, V. S. Padavala and V. R. M. Kolapalli, *Mater. Sci. Semicond. Process.*, 2019, **100**, 301–309.
24 V.-D. Doan, B.-A. Huynh, T.-D. Nguyen, X.-T. Cao, V.-C. Nguyen, T. L.-H. Nguyen, H. T. Nguyen and V. T. Le, *J. Nanomater.*, 2020, **2020**, 1–18.
25 B. Liu, J. Zhuang and G. Wei, *Environ. Sci.: Nano*, 2020, **7**, 2195–2213.
26 H. Van Huan, H. M. Trang and N. Van Toan, *Asian J. Plant Sci.*, 2017, **17**, 56–64.
27 D. N. Dai, T. D. Thang and I. A. Ogunwande, *J. Herbs, Spices Med. Plants*, 2016, **22**, 279–287.
28 V. T. Le, V.-C. Nguyen, X. Cao, T. P. Chau, T. D. Nguyen, T. L. Nguyen and V. Doan, *J. Nanomater.*, 2021, **2021**, 1–11.
29 T. H. A. Nguyen, T. T. V. Le, B. A. Huynh, N. V. Nguyen, V. T. Le, V. D. Doan, V. A. Tran, A. T. Nguyen, X. T. Cao and Y. Vasseghian, *Environ. Res.*, 2022, **212**, 113281.
30 K. Xin Lee, K. Shameli, M. Miyake, N. Kuwano, N. B. Bt Ahmad Khairudin, S. E. Bt Mohamad and Y. P. Yew, *J. Nanomater.*, 2016, **2016**, 1–7.
31 N. Chouhan, R. Ameta and R. K. Meena, *J. Mol. Liq.*, 2017, **230**, 74–84.
32 V. D. Doan, V. S. Luc, T. L. H. Nguyen, T. D. Nguyen and T. D. Nguyen, *Environ. Sci. Pollut. Res.*, 2020, **27**, 6148–6162.
33 M. Annadhasan, T. Muthukumarasamyvel, V. R. Sankar Babu and N. Rajendiran, *ACS Sustainable Chem. Eng.*, 2014, **2**, 887–896.
34 E. Priyadarshini and N. Pradhan, *Sci. Rep.*, 2017, **7**, 1–8.
35 S. Thatai, P. Khurana, S. Prasad, S. K. Soni and D. Kumar, *Microchem. J.*, 2016, **124**, 104–110.
36 E. Tan, P. Yin, X. Lang, H. Zhang and L. Guo, *Spectrochim. Acta, Part A*, 2012, **97**, 1007–1012.
37 X. Mao, Z.-P. Li and Z.-Y. Tang, *Front. Mater. Sci.*, 2011, **5**, 322–328.
38 S. Hu, P. J. J. Huang, J. Wang and J. Liu, *Anal. Chem.*, 2020, **92**, 13354–13360.